



Universiteit
Leiden
The Netherlands

Single-cell mechanical characterization of human macrophages

Evers, T.M.J.; Sheikhhassani, V.; Tang, H.; Haks, M.C.; Ottenhoff, T.H.M.; Mashaghi, A.

Citation

Evers, T. M. J., Sheikhhassani, V., Tang, H., Haks, M. C., Ottenhoff, T. H. M., & Mashaghi, A. (2022). Single-cell mechanical characterization of human macrophages. *Advanced Nanobiomed Research*, 2(7). doi:10.1002/anbr.202100133

Version: Publisher's Version

License: [Creative Commons CC BY 4.0 license](https://creativecommons.org/licenses/by/4.0/)

Downloaded from: <https://hdl.handle.net/1887/3464494>

Note: To cite this publication please use the final published version (if applicable).

Single-Cell Mechanical Characterization of Human Macrophages

Tom M. J. Evers, Vahid Sheikhhassani, Huaqi Tang, Mariëlle C. Haks, Tom H. M. Ottenhoff, and Alireza Mashaghi*

Macrophages remodel their mechanics during differentiation toward different subtypes and drastically adapt their shapes during phagocytosis or entry to inflamed tissues. Although these functions depend on cell mechanical properties, the mechanical behavior of macrophages is still poorly understood and accurate physiologically relevant data on basic mechanical properties of different macrophage subtypes are lacking almost entirely. By combining several complementary single-cell force spectroscopy techniques, whole cell mechanics of M1 (differentiated by granulocyte macrophage colony-stimulating factor [GM-CSF]) and M2 (differentiated by macrophage colony-stimulating factor [M-CSF]) macrophages is systematically analyzed, and it is revealed that M2 macrophages exhibit solid-like behavior, whereas M1 macrophages behave more fluid-like. In addition, the findings indicate that M2 macrophages exhibit increased dynamic motility as compared to M1 macrophages, consistent with their mechanical phenotypes. The technology presented herein can be used to distinguish macrophage subtypes based on their mechanical phenotype, and suggests that mechanical properties of macrophages are linked to their immune function.

including wound healing. These cells are also sensitive to the stiffness and topography of the environment^[4] or strains applied to the tissues.^[5–9] It has been suggested that mechanical properties of macrophages are linked to their immune function.^[10–12] Macrophages are known to be highly heterogeneous, with two major polarized phenotypes, called M1 and M2, with distinct morphologies. Morphology is known to be tightly linked to cell mechanics as well. Macrophages thus remodel their mechanics and morphology during differentiation to different macrophage subtypes, a process that is primed by colony-stimulating factors (CSFs). Alterations in the physical microenvironment often underlie pathophysiological states, and understanding of their effects on macrophage phenotype and function may help provide mechanistic insights into disease pathogenesis. As such, probing the mechanical properties of these

1. Introduction

Macrophages are mechanically active immune cells involved in host pathogen interactions, cancer progression, and metastasis.^[1–3] Macrophages are differentiated from blood monocytes that extravasate from blood vessels into tissues where they home and reside to orchestrate immune responses or homeostatic tissue repair


cells could provide fundamentally important insights into their function in health and disease, and could provide novel biomarker of immune activation and disease.

Single-cell modalities such as atomic force microscopy (AFM), micropipette aspiration (MA), and particle tracking microrheology have been used to characterize the viscoelastic properties of cells, but are low in throughput and are typically not amenable for assessing an ensemble of cells.^[13–15] To acquire here significant statistics, multiple single measurements have to be performed. More importantly, most of the techniques require an open chamber configuration, making it difficult to rapidly change the surrounding environment. Magnetic twisting cytometry (MTC) exerts twisting stress on multiple cells simultaneously using functionalized magnetic microbeads attached to cells,^[16,17] and has been employed to probe macrophage elasticity in response to different biological stimuli.^[10] Acoustic tweezing cytometry (ATC) allows for probing cell mechanical properties *in situ*,^[18,19] and has recently been utilized for mechanical phenotyping of macrophages.^[20] Despite the fact that the application of these techniques in macrophage studies has led to insightful findings, none of these studies distinguished between different macrophage subtypes, and thus, a systematic analysis of whole cell mechanics of M1 and M2 is lacking.

Here, we report the first single-cell mechanical characterization of M1 and M2 human macrophages. We use two complementary techniques, optical tweezers (OT) and acoustic force

T. M. J. Evers, V. Sheikhhassani, H. Tang, A. Mashaghi
Medical Systems Biophysics and Bioengineering
Leiden Academic Centre for Drug Research
Faculty of Mathematics and Natural Sciences
Leiden University
Einsteinweg 55, 2333 CC Leiden, The Netherlands
E-mail: a.mashaghi.tabari@lacdr.leidenuniv.nl

M. C. Haks, T. H. M. Ottenhoff
Department of Infectious Diseases
Leiden University Medical Center
Albinusdreef 2, 2333 ZA Leiden, The Netherlands

 The ORCID identification number(s) for the author(s) of this article can be found under <https://doi.org/10.1002/anbr.202100133>.

© 2022 The Authors. Advanced NanoBiomed Research published by Wiley-VCH GmbH. This is an open access article under the terms of the Creative Commons Attribution License, which permits use, distribution and reproduction in any medium, provided the original work is properly cited.

DOI: 10.1002/anbr.202100133

spectroscopy (AFS), both for the first time, and measure cellular mechanics and dynamics at physiological temperature.

2. Results

2.1. Human Macrophage Mechanics Is Strain Rate Dependent at Low Stretching Velocities

We set out to probe the mechanical properties of primary macrophages at physiological temperature using OT. To do so, freshly isolated monocytes from healthy human blood bank donors were differentiated with granulocyte macrophage colony-stimulating factor (GM-CSF) or macrophage colony-stimulating factor (M-CSF), which are known to prime toward proinflammatory (IL12+) M1 and anti-inflammatory (IL10+) M2 phenotypes, respectively.^[21,22] We observed that M2 macrophages were remarkably larger in size (nonadherent) than M1 macrophages (≈ 17 vs $11 \mu\text{m}$, respectively), as illustrated by the microscopic images in **Figure 1AI** and **II**. Macrophages were clamped between two optically trapped beads and subsequently stretched by displacing one of the trapped beads for 500 nm while keeping the other bead stationary (**Figure 1A**). We performed multiple stretching cycles (**Figure 2A**), in which the cells were pulled at a constant strain rate at different values of the velocity $v = dx/dt$ of $1, 3, 5, 7, 10, 15,$ and $20 \mu\text{m s}^{-1}$. We first determined the stiffness of the cell at the different stretching velocities by linear fits through the obtained force-extension curves.

Importantly, M2 macrophages showed significantly increased stiffness at all applied strain rates as compared to M1 macrophages (**Figure 2C**). Notably, both M1 and M2 macrophages showed a strain-rate dependent increase in stiffness at lower velocities ($1\text{--}7 \mu\text{m s}^{-1}$). In addition to stiffness, we determined the viscoelastic behavior of macrophages by fitting their relaxation response to a power-law decay function (**Figure 2B**), according to

$$F(t) = \Delta F_0 \times \left(\frac{t}{t_0}\right)^{-\beta} + F_{\text{inf}} \quad (1)$$

where $F(t)$ denotes the measured force at time t , ΔF_0 the final force value corresponding to the plateau, β the power-law exponent, and F_{inf} a constant. In the power-law function, a purely elastic solid exhibits a power-law exponent of 0, and a purely viscous fluid exhibits a power-law exponent of 1. We found a significantly lower power exponent for M2 macrophages (0.29 ± 0.04) as compared to M1 macrophages (0.48 ± 0.07).

2.2. M2 Macrophages Are More Viscoelastic than M1 Macrophages

In order to further characterize the viscoelastic properties of M1 and M2 macrophages, we employed AFS, a method that complements OT in experimental throughput, i.e., in OT, only one cell can be manipulated, whereas in AFS, multiple cells can be probed during a single measurement. This technique has recently been employed to probe the mechanical properties of kidney embryonic cells^[23] and human umbilical vein endothelial cells.^[24,25] In our experimental setup, human M1 and M2 macrophages are confined between concanavalin A-functionalized silica beads ($7.9 \mu\text{m}$ in diameter) and the glass surface of the AFS microfluidic chip (**Figure 1B**). Acoustic forces are applied via a piezo element, which generates standing acoustic waves that push the beads up toward the acoustic node, instantaneously stretching the cells at an approximately constant stress σ (**Figure 3A**); in contrast, the OT experiment is considered to expose the cells to a step stress. Bead movement is tracked in real time, where the z -directional displacement corresponds to the elongation of the cell, a quantity directly related to the strain. For our experiments, only beads that are attached on top of cells are included in the analysis, as beads that are attached to the side of a cell might interact with the surface which can affect the results.

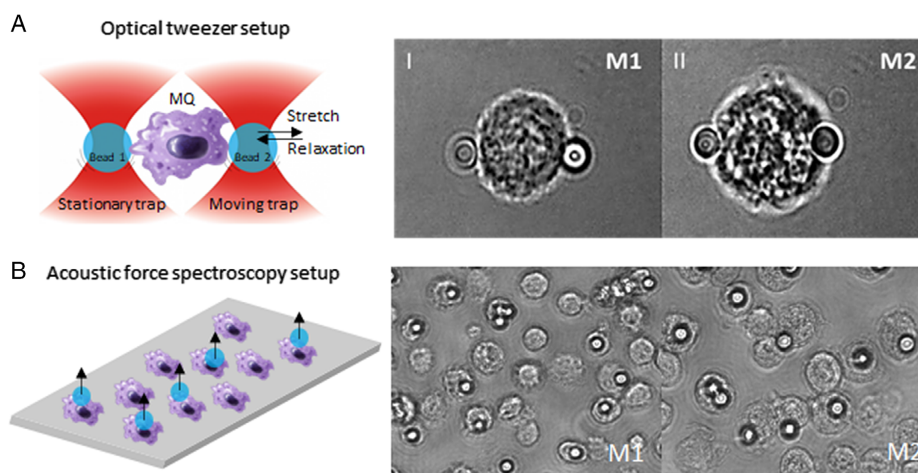


Figure 1. Experimental setups. A) Cartoon representation of the OT microfluidic chip containing a macrophage that is sandwiched between two optically trapped silica beads. (I–II) Microscopic images of an M1 and M2 macrophage, respectively. B) Cartoon representation of the AFS microfluidic chip loaded with macrophages. A standing acoustic wave drives silica beads to the acoustic node thereby stretching the macrophages. Microscopic image of multiple M1 and M2 macrophages with silica beads attached on top.

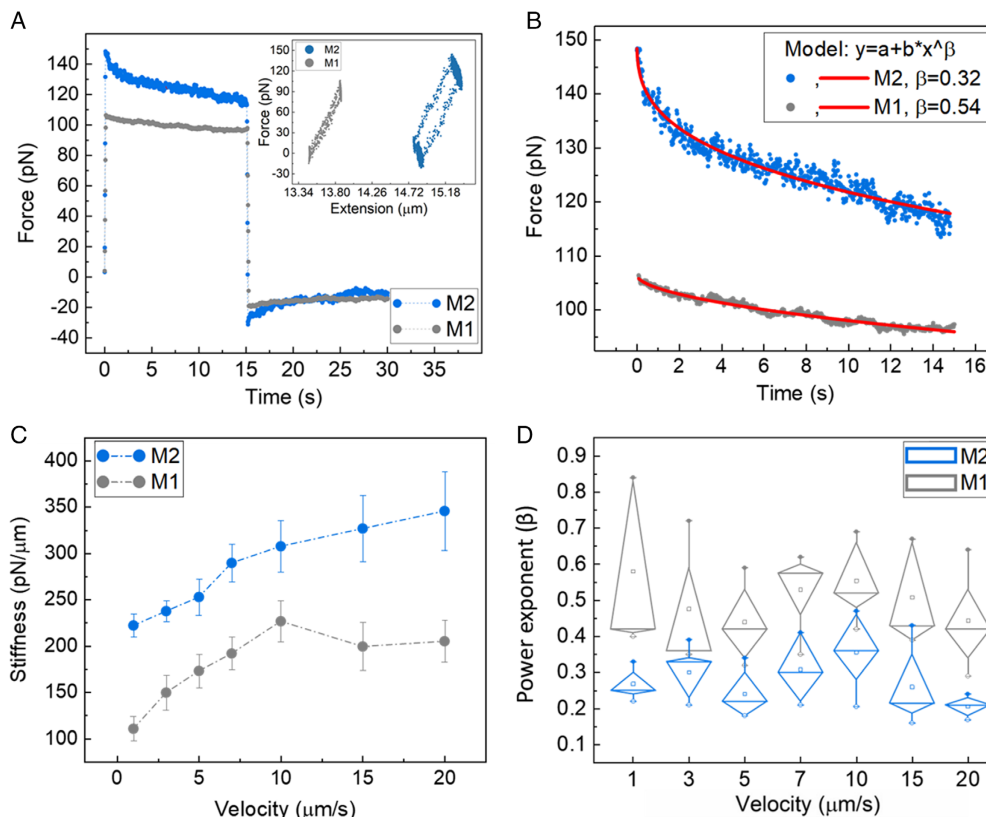


Figure 2. Macrophage mechanics is strain rate dependent. A) Typical trace of measured force as a function of time and inset: force as a function of extension at 10 μm s⁻¹ for M1 and M2 macrophages. B) Typical trace of relaxation force as a function of time fitted by power-law model. C) Dynamic stiffness (mean values) of macrophages at physiological temperature showing significant differences between M1 (*n* = 7) and M2 (*n* = 6) cells at all strain rates (*p* < 0.0001). D) Power exponent of stress relaxation analysis as a function of strain rate showed a significant difference between M1 and M2 macrophages (*p* < 0.0001). Data of several experiments (*n* = at least 2) have been pooled. Violin plot whiskers (mean, median ± SEM) plotted using Tukey's method in Origin-Lab (2019b).

In response to acoustic forces, human macrophages show a typical creep response: an initial regime of sublinear viscoelastic response followed by the slow linear increase characteristic of purely viscous response (Figure 3C). From our stress–strain curves, we first calculated the creep compliance

$$J(t) = \frac{\gamma(t)}{\sigma} = \frac{\Delta d}{\frac{r}{A} F} (t) \quad (2)$$

where γ is the strain estimated as $\Delta d/r$ (r = radius of the silica bead), and σ is the typical stress defined by the applied force F divided by the area of contact between the bead and the cell A , i.e., the total load strain per unit of stress for each macrophage over a time span of 15 s, similar to the time that cells were kept under tension in our OT experiments. From the creep compliance, we determined the viscoelastic properties. While with OT it is possible to apply force on small contact areas and induce local deformation and extrusion of cellular protrusions, our protocol leads to whole cell deformation and thus our study does not include cellular protrusions, which are associated with distinct force profiles. It has previously been described that macrophages

are mechanically best represented by the solid linear liquid (SLL) model,^[26] which places a spring and a dashpot (whose elastic modulus E_a and viscosity η_a we label with the index a to indicate they are associated with the cytoskeleton) in parallel with a background viscous medium (\approx the cytosol) with viscosity η_c (Figure 3B).

Fitting the SLL model to the data, we observed significantly higher average elastic modulus E_a , viscosity η_a , and background viscosity η_c in M2 macrophages as compared to M1 macrophages (Figure 3). Our AFS data are consistent with the OT data, indicating that M2 macrophages are stiffer as compared to M1 macrophages.

2.3. M2 Macrophages Migrate Farther, Faster, and Straighter than M1 Macrophages

The ability of macrophages to migrate is a prerequisite to fulfill their various functions. For instance, the outcome of diseases depends on the balance between the migration/accumulation of proinflammatory M1 and anti-inflammatory M2 macrophages in inflamed tissue. This raises the question whether these cells

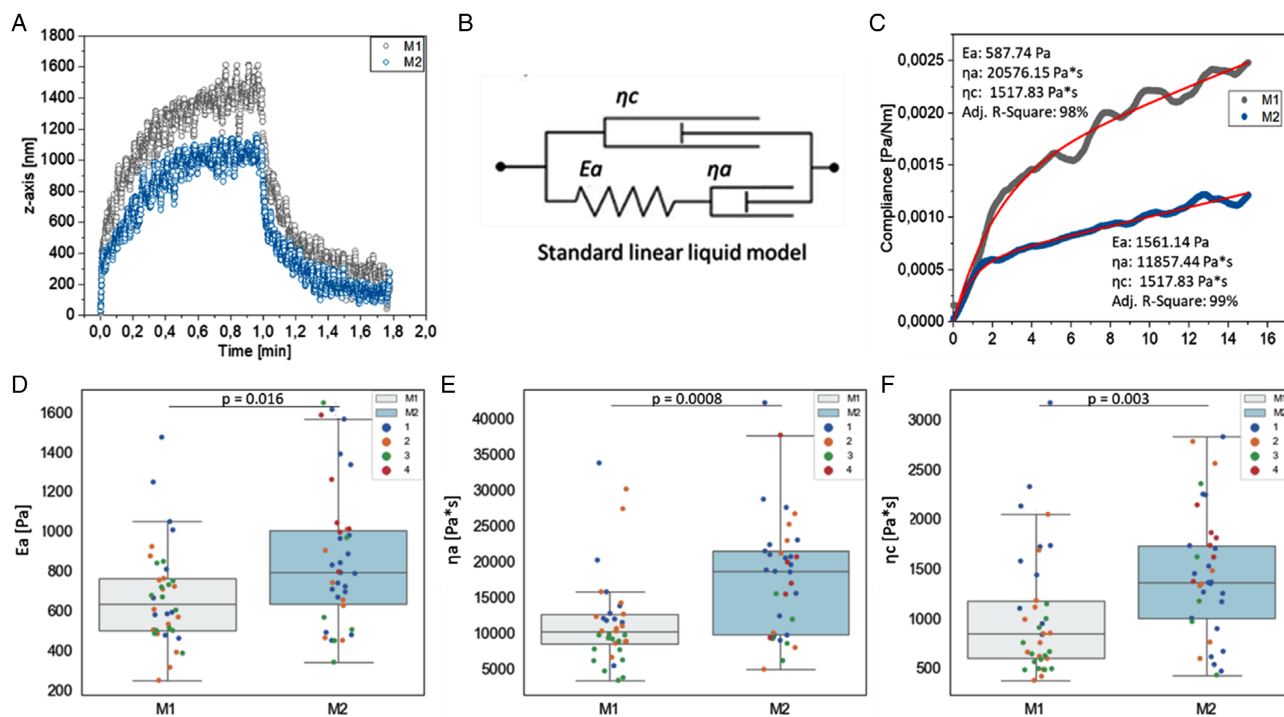


Figure 3. Viscoelastic properties of M1 and M2 macrophages. A) Demonstration of the viscoelastic behavior of an M1 and M2 macrophage upon the application of a constant force step (≈ 3.5 nN). B) Schematic representation of the standard linear liquid model. C) Creep compliance curves of an M1 and M2 macrophages in response to the application of a constant force (≈ 3.5 nN). D) The average elastic modulus E_a is significantly higher in M2 macrophages ($n = 38$) as compared to M1 macrophages ($n = 38$). E) M2 macrophages exhibit a significantly higher mean viscosity η_a as compared to M1 macrophages. F) M2 macrophages exhibit a significantly higher background viscosity η_c as compared to M1 macrophages. Box plot whiskers (median \pm SEM) were plotted in Origin-Lab (2019b). Each dot represents a single cell. Colored dots in boxplots represent different experimental replicates. p -values calculated using Mann–Whitney test.

also show heterogeneity in dynamics. In order to probe macrophage dynamics, M1 and M2 macrophages were seeded and incubated for attachment on a specifically designed migration chip. The migration chip comprises three chambers for parallel assays, and each chamber consists of two large reservoirs connected by a narrow observation area. To track macrophage movement, time-lapse images were taken at a time interval of 10 min for 14 h. Datasets from the Manual Tracking of ImageJ were imported into Chemotaxis and Migration Tool and the cell trajectories were all extrapolated to $(x, y) = 0$ at time 0 h. The migration plot of M1 and M2 macrophages is shown in Figure 4A, in which both macrophage subtypes moved in all directions arbitrarily. Several parameters characterizing macrophage migration are computed from the trajectories, which have been described in detail previously.^[27] Briefly, Euclidian distance is the direct distance between start and end point of a cell track. Accumulated distance is the sum of all incremental movements measured in between all single images. Velocity was computed as the ratio of the accumulated distance and migration time. The directness, which represents a cell's tendency to migrate in a straight line, was calculated by dividing the Euclidian distance by the accumulated distance. M2 macrophages showed significantly higher average velocity, accumulated distance, Euclidian distance, and directness compared to M1 macrophages (Figure 4B). Our

findings indicate the M2 macrophages migrate farther, faster, and straighter than M1 macrophages.

3. Discussion and Conclusion

Our findings present the first single-cell mechanical characterization of GM-CSF differentiated and M-CSF differentiated human macrophages, which we refer to as M1 and M2 macrophages. Our observations indicate that 1) macrophage mechanics is strain rate dependent at low stretching velocities, 2) M2 macrophages are stiffer than M1 macrophages, and 3) M2 macrophages exhibit stronger migratory ability as compared to M1 macrophages.

It is important to note that we characterized the mechanical phenotype of macrophages at physiological temperature, as relevant data on macrophage mechanics under physiological temperatures are largely lacking. Previous studies probed the viscoelastic properties of macrophages either at room temperature or by utilizing cell line models or rodent cells, which do not fully recapitulate human macrophage physiology and functionality. We realize that M1 and M2 differentiated macrophages are simplified models, and macrophages in the circulation or tissues may represent “mixed phenotypes.” However, these two subsets

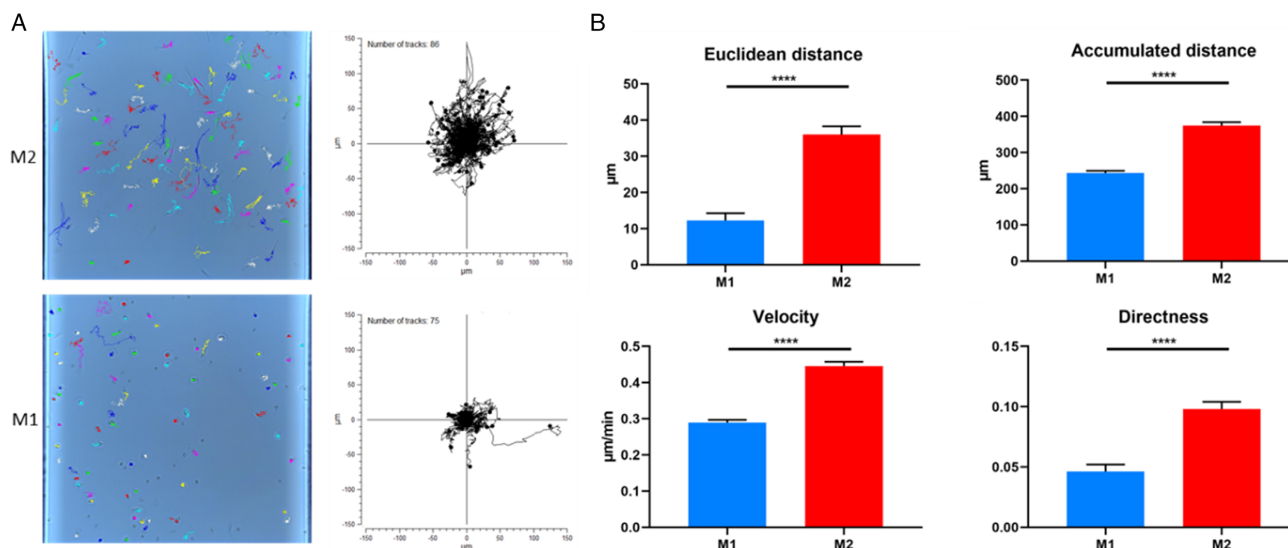


Figure 4. Distinct migratory properties of M1 and M2 macrophages at single-cell resolution. A) M1 and M2 macrophages microscopy images of the chamber observation area with an overlay of the tracked cell trajectories and the corresponding trajectory plot, of which starting point of each single cell is placed in the center of the diagram. B) Comparison of analyzed migration parameters between M1 and M2 macrophages. Results show that M2 macrophages possess much stronger migratory ability compared to M1. Bar plot whiskers (mean ± SEM) were plotted in Origin-Lab (2019b). *p*-values calculated using two-tailed Student's *t*-test (*****p* < 0.0001).

characterize the most variable difference in macrophage functional properties, and therefore, provide a suitable model for analyzing whole cell mechanics in different macrophage subsets.

Recently, we uncovered the importance of monocyte mechanics in their recruitment to sites of infection, by observing that exposure to CCL2—a chemokine and primary mediator in monocyte recruitment—can increase monocyte stiffness and viscous properties, helping them switch to a migration-competent state and progress to sites of infection.^[28] Similarly, in this study, we found that the more migration-competent cells, the M2 macrophages, exhibit increased stiffness as well as viscous properties. This knowledge could, ultimately, provide a novel biomarker for health and disease. The pronounced differences in mechanical properties between M1 and M2 may relate to the key physiological functions of these macrophages. M2-like macrophages have been shown to exhibit higher phagocytic capacity compared to M1-like macrophages.^[29] Micropipette aspiration studies have led to a simple physical model for relocation of the phagosome toward the cell interior in the last step of phagocytosis, involving a balance between membrane tension leading to cell rounding and cytoplasmic viscosity resisting cellular shape change,^[30] which may relate to the higher cytoplasmic viscosity observed in M2 macrophages.

Tissue structure and physical cues in the extracellular environment also contribute to macrophage function. M2-polarized macrophages are most frequently observed within rigid tissue architectures, such as the tumor microenvironment,^[31] and the collagen-rich fibrous cap and adventitia surrounding atherosclerotic plaques.^[32,33] It is well known that tissue or matrix rigidity promotes actin polymerization and cellular stiffening,^[34,35] which would justify higher stiffness in M2 macrophages compared to M1.

Regarding dynamic motility, we performed comparison via a migration chip without coating of surface and this platform has

the capability to automated track label-free cells under phase contrast microscope for long-term experiments. The results here show that M2 macrophages possess much stronger migratory ability than M1 phenotype. These distinct migratory properties between M1 and M2 macrophages may contribute to their opposite biological functions; the primary role of M1 macrophages is to remain at the site of infection, clearing pathogens, and activating adaptive immune responses, which reduces the immediate need to migrate large distances. On the other hand, the increased phagocytic properties of M2 macrophages, coupled with their high migratory abilities, confirm the major function of anti-inflammatory macrophages—phagocytosis followed by efflux from the tissue.

A better understanding of how physiological and diseased microenvironmental cues regulate M1 and M2 macrophage mechanics will be critical for developing immune-targeted therapies for the treatment of many diseases. For example, the presence of M2-like tumor-associated macrophages (TAMs) in tumors has been directly correlated to poor prognosis, and is associated with increased metastatic potential.^[36,37] Recent evidence suggests that TAMs associate with and likely guide cancer cells in migration in a localized manner.^[38] Therefore, therapies may benefit from modulation of macrophage mechanics and limiting their migration.

4. Experimental Section

Macrophage Differentiation: Peripheral blood mononuclear cells (PBMCs) were isolated from buffy coats (Sanquin Blood Bank, Leiden, The Netherlands) collected from healthy anonymous blood bank donors (Dutch, adults) who had signed written informed consent for scientific use of blood products. Research was performed with the approval of the Institutional Review Board of the Leiden University Medical Center,

The Netherlands. The study was conducted in accordance with the most recently revised Declaration of Helsinki. PBMCs were isolated using Ficoll density gradient (Ficoll-Paque, Darmstadt, Germany). Monocytes were isolated from PBMCs by positive selection with a monocytic (using CD14+) MACS microbeads and columns according to the manufacturer's protocol (MiltenyiBiotec, Bergisch Gladbach, Germany). Purity of the CD14+ fraction was assessed with flow cytometric analysis.

Monocytes were cultured at 37 °C/5% CO₂ in Gibco Roswell Park Memorial Institute (RPMI) 1640 (Dutch modified) medium (Life Technologies-Invitrogen, Bleiswijk, The Netherlands) supplemented with 10% FBS, 2 mM L-alanyl-L-glutamine (GlutaMAX) (PAA, Linz, Austria), 100 U mL⁻¹ penicillin, and 100 µg mL⁻¹ streptomycin (Life Technologies-Invitrogen) at a concentration of 1 × 10⁶ cells mL⁻¹ in a T75 culture flask. For differentiation into macrophages, the following concentration of cytokines was added: 5 ng mL⁻¹ GM-CSF (Life Technologies-Invitrogen) for M1 and 50 ng mL⁻¹ M-CSF (R&D Systems, Abingdon, UK) for M2 macrophages.^[21,22] At day 3 of differentiation, new cytokines (same concentrations) were added. At day 6 of differentiation, M1 and M2 macrophages were harvested using Trypsin-EDTA 0.05% (ThermoFisher Scientific) and scraping. The concentration of the macrophage suspensions was adjusted to 1 × 10⁶ cells mL⁻¹ to ensure optimal working coverage of the chip, whereas OT required a significantly lower concentration.

Silica Microbead Functionalization: Silica microbeads were functionalized according to the protocol described by Sorokin et al.,^[39] with minor modifications. Briefly, silica microbeads (7.9 and 4.1 µm in diameter for AFS and OT respectively, 1% w/w; Spherotech, Inc.) were first washed by 3% v/v dilution in PBS, followed by centrifugation at 2000 RPM (for 3 min) and removal of supernatant. Then, microbeads were surface activated by incubation in 3% HCl (10 min). After washing in PBS and centrifugation at 2000 RPM for 3 min (2 ×), microbeads were functionalized by incubation with concanavalin A (1 mg mL⁻¹; Sigma-Aldrich C5275) for 30 min at 4 °C using a tube rotator. Finally, the microspheres were washed and resuspended in 500 µL PBS.

OT Force Spectroscopy Experiments: In our OT experimental setup, macrophages were sandwiched between two separate concanavalin A (ConA)-coated silica beads (≈4 µm, silica beads, Bangs-lab). Both beads were optically trapped and macrophages were kept at least 4 µm away from the glass surface in order to prevent possible effects of hydrodynamic forces on cell mechanics. The traps were calibrated at physiological temperature before attaching the beads to the cell, for each set of measurements. Notably, the sizes of the trapped beads were chosen so that the cell was not directly exposed to the laser beam, even in the most displaced position (diameter of focused laser beam at the center of the trap was less than 800 nm).

Force spectroscopy measurements were conducted in a cyclic manner, in which the macrophage was periodically stretched, followed by a relaxation time. More specifically, the manipulation cycle consisted of four separate steps: step 1 (stretch): the macrophage was stretched by moving one of the traps with a preknown velocity for 500 nm (constant strain). Step 2 (relaxation): the macrophage relaxed the exerted tension and reached mechanical equilibrium (15 s). Step 3 (retraction): the displaced trap was returned to its initial position at the same velocity used in step 1. Step 4 (relaxation): traps were kept stationary for over 15 s to let the macrophages relax, again. All measurements were conducted using a C-trap (Lumicks B.V., Amsterdam) OT machine. The OT machine was equipped with an IR laser source with wavelength of λ = 1064 nm implemented in an inverted microscope. For all measurements, laser power was precisely set to 500 mW on each laser beam trapping a 4 µm bare silica beads. For tracking the beads at high frequency, piezo tracking module of the BlueLake software, commercially available through the manufacturing company, was used.

AFS Experiments: Details on AFS setup, specifications, and fabrication have been provided in earlier publications.^[39,40] All measurements were conducted using AFS-G2 from Lumicks B.V., which comprises a motorized z-stage mounted on an inverted Nikon microscope (Eclipse, TE200), G2 AFS chip holders (microfluidic devices), and a temperature controller. Macrophages were injected into the microfluidic chamber of the AFS chip, which is mounted on the AFS microscope setup. The cells were incubated

for approximately 1 min, in which they precipitate and adhere to the bottom glass surface. After removal of unattached cells, new macrophages were injected until a desired number of cells adhered to the surface inside the calibrated field of view. Next, silica microbeads (7.9 µm in diameter, Spherotech, Inc., SIP-60-10) functionalized with Con-A were introduced into the microfluidic chamber, and randomly attached on top of macrophages. Con-A is a lectin and binds to carbohydrates residues on the cell surface. Beads were tracked using the LabVIEW software provided by Lumicks B.V. (Amsterdam, The Netherlands). Particle z-position was determined by a look-up-table (LUT), set to track from 0 to 10 000 nm at a step size of 100 nm. After generating the LUT for each individual bead in the field of view, constant acoustic forces were applied, pulling the beads upward, thereby stretching the macrophages. For determination of the viscoelastic properties of human macrophages, force clamps ranging from 1.8 to 3.5 nN (50–70%, 14.37 MHz) were used for further analysis. All experiments were conducted at physiological temperature.

Determining the Viscoelastic Properties of M1 and M2 Macrophages: The viscoelastic properties were determined by fitting to the standard linear liquid (SLL) model. The creep compliance $J(t)$, as a function of time, in the SLL model is given by

$$J(t) = \left(\frac{t}{\eta_a + \eta_c} \right) + \left(\frac{\eta_a^2}{E_a(\eta_a + \eta_c)^2} \right) * \left(1 - e^{-\left(\frac{t}{\eta_a + \eta_c} \right)} \right) \quad (3)$$

where E_a is the elasticity associated with the actin cytoskeleton, η_a is the viscosity associated with the cytoskeleton, and η_c is the background viscosity.

The extension curves, z-height versus time, were first converted to $J(t)$, where

$$J(t) = \frac{\gamma}{\sigma} \quad (4)$$

where γ is the strain estimated as $\Delta d/r$ (r = radius of the silica bead), and σ is the typical stress defined by the applied force (1.8–3.5 nN) divided by the area of contact between the bead and the cell. $J(t)$ was then plotted as a function of time and Equation (3) was fit to the resultant curves. The Origin-Lab fitting tool was used to automatically fit standard linear liquid model to all measured compliance versus time plots.

Live Single-Cell Migration Assay: Cell migration assays were performed using the µ-Slide Chemotaxis (80326, ibidi GmbH) according to the manufacturer's protocol.^[41,42] Briefly, cell suspension (6 µL) of 3 × 10⁶ cells mL⁻¹ were seeded into the center chamber of a µ-Slide. After cell adhesion, the two opposing reservoirs were filled with culture medium containing 10% FBS. Cell migration was recorded every 10 min for overnight by mounting the µ-Slide on the stage of a Nikon Eclipse Ti inverted microscope with a 37 °C incubator and 5% CO₂. Single-cell tracking and analysis in the observation area of each image sequence were done using the Manual Tracking plugin of ImageJ and ibidi Chemotaxis and Migration Tool (version 2.0).

Statistical Analysis: Normality of the data sets was tested with a Shapiro–Wilk normality test. For data sets that were normally distributed, a two-sample t-test was used. For datasets that were not normally distributed, the nonparametric Mann–Whitney U test was employed. For OT data sets, ANOVA was used to determine significant differences between applied strain rates. Data are taken as significant if the p-value is lower than 0.05. For data processing and visualization, Python (version 2.7.15) and Origin (version 2019b) were utilized.

Acknowledgements

T.M.J.E. and V.S. contributed equally to this work. A.M., T.M.J.E., and H.T. thank the Netherlands Organization for Scientific Research (NWO-TTW, grant no. 16249). H.T. was financially supported by the CSC Scholarship offered by the China Scholarship Council. T.H.M.O. acknowledges the Netherlands Organization for Scientific Research (NWO-TOP grant agreement no. 91214038).

Conflict of Interest

The authors declare no conflict of interest.

Data Availability Statement

The data that support the findings of this study are available from the corresponding author upon reasonable request.

Keywords

acoustic force spectroscopy, macrophages, optical tweezers, single-cell mechanics, single-cell migration

Received: October 14, 2021

Revised: April 11, 2022

Published online: April 28, 2022

- [1] X. Zhang, T. H. Kim, T. J. Thauland, H. Li, F. S. Majedi, C. Ly, Z. Gu, M. J. Butte, A. C. Rowat, S. Li, *Curr. Opin. Biotechnol.* **2020**, *66*, 236.
- [2] N. Jain, J. Moeller, V. Vogel, *Annu. Rev. Biomed. Eng.* **2019**, *21*, 267.
- [3] V. S. Meli, P. K. Veerasubramanian, H. Atcha, Z. Reitz, T. L. Downing, W. F. Liu, *J. Leukocyte Biol.* **2019**, *106*, 283.
- [4] S. Chen, J. A. Jones, Y. Xu, H. Y. Low, J. M. Anderson, K. W. Leong, *Biomaterials* **2010**, *31*, 3479.
- [5] J. Pugin, I. Dunn, P. Jolliet, D. Tassaux, J. L. Magnenat, L. P. Nicod, J. C. Chevrolet, *Am. J. Physiol. - Lung Cell. Mol. Physiol.* **1998**, *275*, L1040.
- [6] K. Kurata, T. Uemura, A. Nemoto, T. Tateishi, T. Murakami, H. Higaki, H. Miura, Y. Iwamoto, *J. Bone Miner. Res.* **2001**, *16*, 722.
- [7] V. Ballotta, A. Driessen-Mol, C. V. C. Bouten, F. P. T. Baaijens, *Biomaterials* **2014**, *35*, 4919.
- [8] A. G. Solis, P. Bielecki, H. R. Steach, L. Sharma, C. C. D. Harman, S. Yun, M. R. de Zoete, J. N. Warnock, S. D. F. To, A. G. York, M. Mack, M. A. Schwartz, C. S. Dela Cruz, N. W. Palm, R. Jackson, R. A. Flavell, *Nature* **2019**, *573*, 69.
- [9] N. Jain, V. Vogel, *Nat. Mater.* **2018**, *17*, 1134.
- [10] N. R. Patel, M. Bole, C. Chen, C. C. Hardin, A. T. Kho, J. Mih, L. Deng, J. Butler, D. Tschumperlin, J. J. Fredberg, R. Krishnan, H. Koziel, *PLoS One* **2012**, *7*, e41024.
- [11] E. F. Irwin, K. Saha, M. Rosenbluth, L. J. Gamble, D. G. Castner, K. E. Healy, *J. Biomater. Sci., Polym. Ed.* **2008**, *19*, 1363.
- [12] T. H. Kim, C. Ly, A. Christodoulides, C. J. Nowell, P. W. Gunning, E. K. Sloan, A. C. Rowat, *FASEB J.* **2019**, *33*, 3997.
- [13] J. L. MacKay, S. Kumar, *Cell Imaging Techniques* **2012**, 313.
- [14] D. Kirmizis, S. Logothetidis, *Int. J. Nanomed.* **2010**, *5*, 137.
- [15] A. C. Rowat, in *Physical Properties of the Nucleus Studied by Micropipette Aspiration*, Humana Press, Totowa, NJ **2008**, pp. 3–12.
- [16] F. Chowdhury, S. Na, D. Li, Y. C. Poh, T. S. Tanaka, F. Wang, N. Wang, *Nat. Mater.* **2010**, *9*, 82.
- [17] N. Wang, J. P. Butler, D. E. Ingber, *Science* **1993**, *260*, 1124.
- [18] Z. Fan, Y. Sun, D., . Chen, D. Tay, W. Chen, C. X. Deng, J. Fu, *Sci. Rep.* **2013**, *3*, 2176.
- [19] D. Chen, Y. Sun, M. S. R. Gudur, Y. S. Hsiao, Z. Wu, J. Fu, C. X. Deng, *Biophys. J.* **2015**, *108*, 32.
- [20] X. Hong, P. M. Rzeczycki, R. K. Keswani, M. D. Murashov, Z. Fan, C. X. Deng, G. R. Rosania, *Sci. Rep.* **2019**, *9*, 5702.
- [21] F. A. W. Verreck, T. De Boer, D. M. L. Langenberg, M. A. Hoeve, M. Kramer, E. Vaisberg, R. Kastelein, A. Kolk, R. De Waal-Malefyt, T. H. M. Ottenhoff, *Proc. Natl. Acad. Sci. U.S.A.* **2004**, *101*, 4560.
- [22] F. A. W. Verreck, T. de Boer, D. M. L. Langenberg, L. van der Zanden, T. H. M. Ottenhoff, *J. Leukocyte Biol.* **2006**, *79*, 285.
- [23] V. Romanov, G. Silvani, H. Zhu, C. D. Cox, B. Martinac, *Small* **2021**, *17*, 2005759.
- [24] G. Silvani, V. Romanov, C. D. Cox, B. Martinac, *Front. Bioeng. Biotechnol.* **2021**, *9*, 612151.
- [25] A. Nguyen, M. Brandt, T. Betz, *Lab Chip.* **2021**, *21*, 1929.
- [26] A. E. Ekpenyong, G. Whyte, K. Chalut, S. Pagliara, F. Lautenschläger, C. Fiddler, S. Paschke, U. F. Keyser, E. R. Chilvers, J. Guck, *PLoS One* **2012**, *7*, e45237.
- [27] P. Zengel, A. Nguyen-Hoang, C. Schildhammer, R. Zantl, V. Kahl, E. Horn, *BMC Cell Biol.* **2011**, *12*, <https://doi.org/10.1186/1471-2121-12-21>.
- [28] T. M. J. Evers, V. Sheikhhassani, M. C. Haks, C. Storm, T. H. M. Ottenhoff, A. Mashaghi, *iScience* **2022**, *25*, 103555.
- [29] D. Schulz, Y. Severin, V. R. T. Zanotelli, B. Bodenmiller, *Sci. Rep.* **2019**, *9*, 1925.
- [30] D. Vorselen, R. L. D. Labitigan, J. A. Theriot, *Curr. Opin. Cell Biol.* **2020**, *66*, 112.
- [31] S. Aras, M. Raza Zaidi, *Br. J. Cancer* **2017**, *117*, 1583.
- [32] J. L. Stöger, M. J. J. Gijbels, S. van der Velden, M. Manca, C. M. van der Loos, E. A. L. Biessen, M. J. A. P. Daemen, E. Lutgens, M. P. J. de Winther, *Atherosclerosis* **2012**, *225*, 461.
- [33] G. Chinetti-Gbaguidi, M. Baron, M. A. Bouhrel, J. Vanhoutte, C. Copin, Y. Sebti, B. Derudas, T. Mayi, G. Bories, A. Tailleux, S. Haulon, C. Zawadzki, B. Jude, B. Staels, *Circ. Res.* **2011**, *108*, 985.
- [34] B. L. Doss, M. Pan, M. Gupta, G. Greci, R. M. Mège, C. T. Lim, M. P. Sheetz, R. Voituriez, B. Ladoux, *Proc. Natl. Acad. Sci. U.S.A.* **2020**, *117*, 12817.
- [35] S. Y. Tee, J. Fu, C. S. Chen, P. A. Janmey, *Biophys. J.* **2011**, *100*, L25.
- [36] C. E. Lewis, J. W. Pollard, *Cancer Res.* **2006**, *66*, 605.
- [37] M. Yang, D. McKay, J. W. Pollard, C. E. Lewis, *Cancer Res.* **2018**, *78*, 5492.
- [38] G. Luthria, R. Li, S. Wang, M. Prytskach, R. H. Kohler, D. A. Lauffenburger, T. J. Mitchison, R. Weissleder, M. A. Miller, *Nat. Commun.* **2020**, *11*, 3521.
- [39] R. Sorkin, G. Bergamaschi, D. Kamsma, G. Brand, E. Dekel, Y. Ofir-Birin, A. Rudik, M. Gironella, F. Ritort, N. Regev-Rudzik, W. H. Roos, G. J. L. Wuite, *Mol. Biol. Cell* **2018**, *29*, 2005.
- [40] D. Kamsma, R. Creighton, G. Sitters, G. J. L. Wuite, E. J. G. Peterman, *Methods* **2016**, *105*, 26.
- [41] L. Tomasova, Z. Guttenberg, B. Hoffmann, R. Merkel, *PLoS One* **2019**, *14*, e0219708.
- [42] V. Biswenger, N. Baumann, J. Jürschick, M. Häckl, C. Battle, J. Schwarz, E. Horn, R. Zantl, *PLoS One* **2018**, *13*, e0203040.